2014 IEEE International Conference on Robotics & Automation (ICRA)
Hong Kong Convention and Exhibition Center
May 31 - June 7, 2014. Hong Kong, China

Compliant Control of the Body Shape of Snake Robots

Pål Liljebäck, Kristin Y. Pettersen, Øyvind Stavdahl, and Jan Tommy Gravdahl

***Abstract*— This paper presents a general motion planning framework for body shape control of snake robots. We demonstrate the applicability of the framework for straight line path following control, and for implementing body shape compliance in environments with obstacles. Compliance is achieved by assigning mass-spring-damper dynamics to the shape curve defining the motion of the robot. The performance of the control strategies is illustrated with simulation results.**

I. Introduction

Snake robots are robotic mechanisms designed to move like biological snakes [1]. Their flexible body and narrow cross-section provide traversability in challenging environments which surpasses the mobility of more conventional wheeled, tracked and legged robots.

Numerous approaches to motion control of snake robots have been proposed in the literature, and the reader is referred to [2] for a detailed overview. The majority of previous control approaches are based on specifying directly the motion of each individual joint angle of the snake robot, which means that the overall body shape motion is controlled implicitly through the joint angles (see e.g. [3]–[5]). This approach works well during motion on flat surfaces. In cluttered and irregular environments, however, where adaptation of the motion to the environment is essential in order to maintain mobility, we are primarily interested in controlling the overall (macroscopic) body shape with respect to the environment. For this reason, it would simplify the control problem if we could specify the motion in terms of parameters which are more intuitively mapped to the overall body shape of the snake robot.

To this end, we propose in this paper a motion planning framework for snake robots. Instead of specifying joint angles, the framework allows the motion of the robot to be specified in terms of coordinates of *shape control points* (SCPs). The proposed approach is simple and general, and can also be employed to control flexible robot manipulators.

The applicability of the framework is demonstrated in two steps. In the first step, we employ the framework to formulate a straight line path following controller for snake robots. In the second step, we show how the framework can implement body shape compliance in order to adapt the locomotion in cluttered obstacle environments. The compliance is achieved by assigning mass-spring-damper dynamics to the shape control points, which is a novel approach with respect to previous literature on locomotion control in non-flat environments (see e.g. [6]–[9]).

The framework builds on and improves preliminary results presented in [10], where the authors proposed a similar framework with a different and significantly more complex set of parameters.

The paper is organized as follows. Section II presents a model of the snake robot dynamics in order to introduce basic notation. The general motion planning framework is presented in Section III, and its applicability for path following and body compliance control is demonstrated in Section IV and V, respectively. Simulation results are presented in Section VI, followed by concluding remarks in Section VII.

II. A Mathematical Model of a Snake Robot

This section summarizes a mathematical model of a snake robot crawling on a flat surface with circular obstacles. The model is presented to introduce the notation used in subsequent sections, and has been used to produce the simulation results presented in Section VI. A more detailed presentation of the model is given in [2], [11].

Remark 1: The general motion planning framework presented in this paper yields for three-dimensional motion. For the sake of simplicity, however, the control strategies proposed based on the framework, and therefore also the mathematical model presented in this section, assume that the snake robot carries out planar motion in the horisontal plane.

We consider the snake robot illustrated in Fig. 1, which consists of N links of length l with equal mass m and moment of inertia J. The links are interconnected by $N-1$ motorized joints and the actuator torque at joint $i \in \{1,\dots,N-1\}$ is u_i. Each link is subjected to an isotropic Coulomb ground friction force with friction coefficient μ. The position of the CM (center of mass) of the robot is denoted by $\boldsymbol{p} = (p_x, p_y) \in \mathbb{R}^2$ and the absolute angle θ_i of link $i \in \{1,\dots,N\}$ is expressed with respect to the global x axis with counterclockwise positive direction. The angle of joint i is defined as $\phi_i = \theta_i - \theta_{i+1}$ and the global frame heading of the robot is defined as the average of the link angles, i.e. as $\overline{\theta} = \frac{1}{N}\sum_{j=1}^{N}\theta_j$.

The planar environment of the snake robot contains obstacles with a circular shape. The interaction with an obstacle is modelled by introducing a unilateral velocity constraint for a contacted link. The constraint is *unilateral* (acts in one lateral direction only) since the constraint shall allow sideways motion of the link *away* from the obstacle, but prevent any sideways motion *towards* (and thereby into) the obstacle (see [11] for details). As shown in Fig. 1, the total force from an obstacle on link i consists of an obstacle friction force $\boldsymbol{f}_{\mu,i}$ in the direction parallel to the link and

Affiliation of Pål Liljebäck is shared between the Dept. of Engineering Cybernetics at the Norwegian University of Science and Technology (NTNU), 7491 Trondheim, Norway, and SINTEF ICT, Dept. of Applied Cybernetics, 7465 Trondheim, Norway. E-mail: Pal.Liljeback@itk.ntnu.no.

Kristin Y. Pettersen is with the Centre for Autonomous Marine Operations and Systems, Dept. of Engineering Cybernetics at NTNU, 7491 Trondheim, Norway. E-mail: Kristin.Y.Pettersen@itk.ntnu.no.

Øyvind Stavdahl and Jan Tommy Gravdahl are with the Dept. of Engineering Cybernetics at NTNU, 7491 Trondheim, Norway. E-mail: {Oyvind.Stavdahl, Tommy.Gravdahl}@itk.ntnu.no.

This work was partly supported by the Research Council of Norway through project no. 205622 and its Centres of Excellence funding scheme project no. 223254.

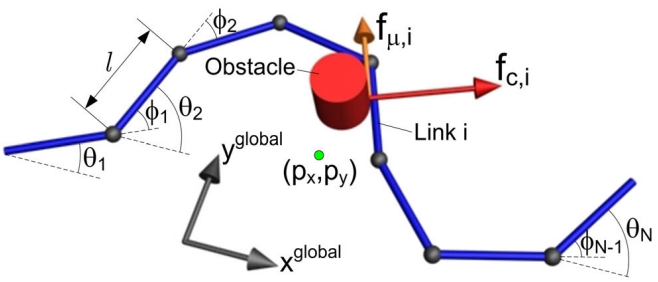

Fig. 1. Parameters of the robot kinematics and obstacle contact forces.

TABLE I
THE BASIC PARAMETERS OF THE MOTION PLANNING FRAMEWORK.

Symbol	Description
n	Number of SCPs in the shape curve.
$\boldsymbol{P}_i \in \mathbb{R}^3$	Coordinates of the ith SCP.
$\boldsymbol{S}(s) \in \mathbb{R}^3$	Shape curve which interconnects the SCPs.
$s_{\text{head}} \in \mathbb{R}$	Shape curve location of the VSR's head.

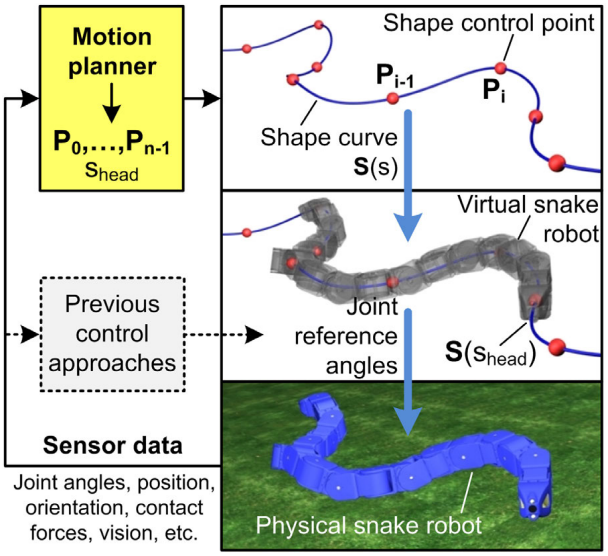

Fig. 2. Overview of the motion planning framework.

an obstacle constraint force $\boldsymbol{f}_{c,i}$ in the normal direction of the link. The magnitude of the obstacle friction force $\boldsymbol{f}_{\mu,i}$ is scaled by the normal force $\boldsymbol{f}_{c,i}$ through the Coulomb friction coefficient μ_o.

III. A Motion Planning Framework for Snake Robot Locomotion

In this section, we propose a general framework which facilitates motion planning for snake robots.

A. Overview of the Motion Planning Framework

The motion planning framework is summarized in Fig. 2. In particular, the desired shape of the snake robot is specified in terms of *shape control points* (hereafter denoted SCPs). The SCPs are interconnected by a curve denoted the *shape curve*, which defines the macroscopic shape of the snake robot. A *virtual snake robot* (hereafter denoted VSR) with identical kinematic structure as the physical robot is aligned along the shape curve, starting from some specified location along the curve. The joint reference angles for the physical robot are then defined as the joint angles of the VSR. Furthermore, dynamic motion patterns for the physical robot are produced by varying the SCP coordinates and/or the location of the VSR along the shape curve with time.

As illustrated in Fig. 2, motion planning is carried out within this framework by specifying the Cartesian coordinates of the SCPs and the shape curve location of the VSR. Whereas previous control approaches are based on specifying the motion of the joints directly (as depicted in Fig. 2), the reference angles within the framework follow implicitly from the explicitly specified body shape since the framework automatically aligns the VSR along the shape curve. Moreover, the task of adapting the body shape motion to the environment is reduced to the task of specifying coordinates of the SCPs in the environment of the robot.

The details of the motion planning framework are now presented using the parameters listed in Table I.

B. The Shape Control Points and the Shape Curve

To construct the shape curve defining the desired shape of the snake robot, we begin by defining a set of SCPs. The global frame coordinates of the SCPs are denoted by $\boldsymbol{P}_0, \boldsymbol{P}_1, \ldots, \boldsymbol{P}_{n-1}$, where n is the number of SCPs in the shape curve and $\boldsymbol{P}_i = [P_{i,x}, P_{i,y}, P_{i,z}]^T \in \mathbb{R}^3$. The number n of SCPs is generally not fixed since the motion of the snake robot can be defined by periodically extending the shape curve with SCPs according to the desired motion pattern.

The shape curve interconnecting the SCPs is denoted by $\boldsymbol{S}(s)$, where $s \in [0, n-1]$ is the scalar shape curve parameter. The curve is produced by interpolating between the SCPs using any chosen interpolation method such that $\boldsymbol{S}(i) = \boldsymbol{P}_i$, where $i \in \{0, \ldots, n-1\}$. Note that motion planning strategies for the SCPs can be specified independently from the choice of interpolation.

Remark 2: Note that the framwork supports locomotion in three-dimensional environments (since the SCPs are defined in $\mathbb{R}^3$), although the control strategies presented in Section IV and V consider planar motion.

C. The Virtual Snake Robot (VSR)

As illustrated in Fig. 2, the shape curve is mapped to joint reference angles for the physical snake robot by aligning a VSR (with identical kinematic structure as the physical robot) along the curve and then using the resulting joint angles of the VSR as reference angles for the physical robot. The motion planner only needs to specify the location of the VSR's head tip on the shape curve, which is denoted by s_{head}. The alignment of the VSR is subsequently carried out automatically within the framework.

Remark 3: The framework does not specify *how* to align the VSR along the shape curve since this is a completely decoupled control problem which depends on the specific kinematic structure of the robot. This decoupling is a significant advantage of the framework since it allows control strategies to be specified on the (macroscopic) shape curve level without considering the specific kinematic structure of

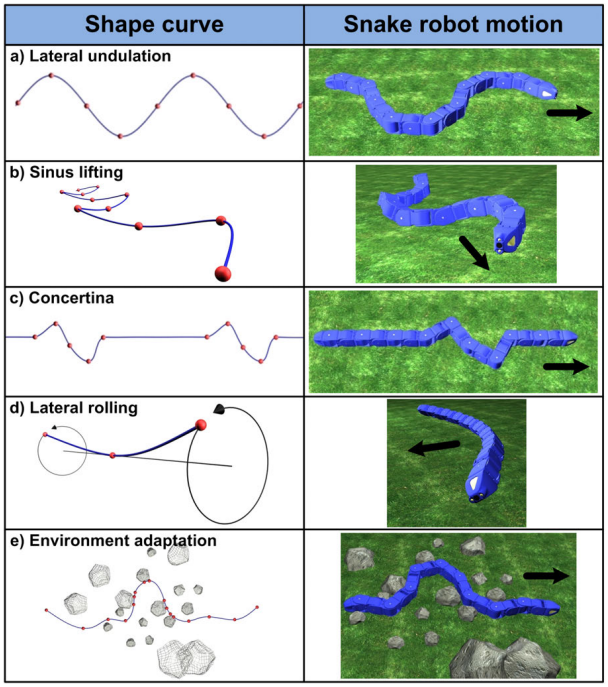

Fig. 3. Examples of applications of the motion planning framework.

the robot (number of joints, length of links, etc.). This also means that the same control strategy can be used to control snake robots with different kinematics.

D. Generating Motion Patterns

Motion patterns are defined by the way the SCP coordinates and/or the location of the VSR along the shape curve are varying with time. There are three possible approaches for generating motion patterns:

1) Progressing the VSR forward along the shape curve while continuously retrieving its joint angles (exemplified in rows (a) - (c) in Fig. 3).
2) Fixing the VSR on the shape curve while varying the SCP coordinates with time (exemplified in row (d) in Fig. 3).
3) A combination of approaches 1 and 2 (exemplified in row (e) in Fig. 3).

Approach 1 is exemplified in rows (a) - (c) in Fig. 3, which show the shape curve for some common locomotion gaits, i.e. *lateral undulation*, *sinus lifting*, *sidewinding*, and *concertina* motion, respectively [2]. Approach 2 is exemplified in row (d) in Fig. 3, where a sideways rolling motion is achieved by fixing the VSR on a shape curve consisting of three SCPs while moving the first and last SCP in a circle. Approach 3 is exemplified in row (e) in Fig. 3, where the SCPs are specified in a map of the environment around the robot. The VSR is progressed forward along the shape curve to create a travelling wave that propels the physical robot forward. At the same time, the SCP coordinates are continuously adjusted based on measured contact forces along the robot body in order to adapt the motion to the environment. This example corresponds to the the control strategy simulated in Section VI.

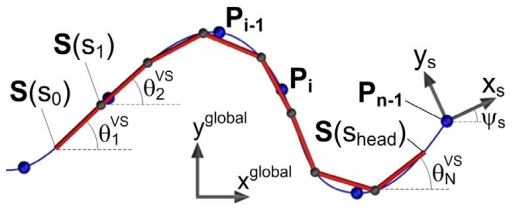

Fig. 4. Parameters of the shape frame and of the VSR aligned along the shape curve.

IV. Application of the Motion Planning Framework for Path Following Control on Flat Surfaces

In this section, we employ the motion planning framework to formulate a path following controller. In Section V, this controller is extended to additionally make the body shape compliant with respect to its environment.

A. Assumptions

Although the motion planning framework supports locomotion in three-dimensional environments (since the SCPs are defined in $\mathbb{R}^3$), we assume that the robot undergoes strictly planar motion according to the model presented in Section II. The measured sensor data available to the controller are the CM position (p_x, p_y), the heading $\overline{\theta}$, and the joint angles ϕ_j, $j \in \{1, \ldots, N-1\}$, of the physical snake robot.

Remark 4: If the path following controller is employed on a flat surface, the links must have *anisotropic* friction properties in order for the ground friction forces to efficiently propel the robot [2]. In obstacle environments, on the other hand, the links may have *isotropic* friction properties since obstacles can be used as push-points in order to propel the robot. We call this *obstacle-aided locomotion* [2].

B. The Control Objective

The control objective is to steer the robot so that it converges to and tracks a straight path while maintaining a heading parallel to the path. To this end, we define the global frame so that the global x axis is aligned with the desired straight path. The position of the snake robot along the global y axis, p_y, is then its distance to the desired path (i.e. the cross-track error) and the heading $\overline{\theta}$ is its angle with respect to the path.

C. The Path Following Controller

The complete path following controller is detailed in this subsection. In addition to the basic framework parameters listed in Table I, the controller also makes use of the parameters illustrated in Fig. 4 and listed in Table II (where we have included model parameters from Section II).

1) The Gait Segment: We choose to propel the snake robot according to the gait pattern *lateral undulation* [2]. This gait pattern is the most common form of snake locomotion and consists of travelling waves that are propagated backwards along the body in order to propel the robot forward. We achieve this motion pattern by defining a *gait segment*

TABLE II
PARAMETERS OF THE PATH FOLLOWING CONTROLLER.

Symbol	Description
N	Number of snake robot links.
l	Length of each snake robot link.
$p_x, p_y \in \mathbb{R}$	CM position of the *physical* robot.
$\phi_j \in \mathbb{R}$	Angle of joint j of the *physical* robot.
$u_j \in \mathbb{R}$	Actuator torque at joint j of the *physical* robot.
k_p, k_d	Joint angle controller gains of the *physical* robot.
$\overline{\theta}, \overline{\theta}^{\text{VS}} \in \mathbb{R}$	Heading of the *physical* robot and the VSR.
$\theta_j, \theta_j^{\text{VS}} \in \mathbb{R}$	Angle of link j of the *physical* robot and the VSR.
$s_j \in \mathbb{R}$	Shape curve location of joint j of the VSR.
$v^{\text{VS}} \in \mathbb{R}$	Velocity of the VSR along the shape curve.
k	Number of SCPs in the gait segment.
$\boldsymbol{P}_i^{\text{GS}} \in \mathbb{R}^3$	Coordinates of the ith SCP in the gait segment.
$\psi_s \in \mathbb{R}$	Angle of the shape frame wrt the global frame.
$k_\psi, \Delta \in \mathbb{R}$	Heading controller gain and look-ahead distance.

according to a single period of the cyclic wave motion. The gait segment is simply a collection of k SCPs denoted by

$$\left\{ \boldsymbol{P}_0^{\text{GS}}, \boldsymbol{P}_1^{\text{GS}}, \ldots, \boldsymbol{P}_{k-1}^{\text{GS}} \right\} \tag{1}$$

which defines the form of the shape curve over *one* cycle of the motion pattern, and where superscript 'GS' is short for *gait segment*. The segment is repeatedly concatenated with the shape curve *one* SCP at a time to create a cyclic motion. We only add *one* SCP at a time since this allows for directional control of the motion each time a new SCP is added (see Section IV-C.4).

Note that the framework gives us the freedom to 'draw' any type of wave shape using the SCP coordinates in (1), such as a rectangular or sinusoidal shape with a desired amplitude and wave length. As an example, Fig. 8(a) shows the specific gait segment used to simulate the path following controller in Section VI.

2) The Shape Frame: In order to control the direction in which the shape curve is developed, we define, as shown in Fig. 4, a *shape frame* with coordinate axes denoted by x_s and y_s, respectively. The angle between the global x axis and the x_s axis is denoted by ψ_s. Furthermore, the origin of the shape frame coincides with the last SCP of the shape curve, whose coordinates are $\boldsymbol{P}_{n-1} = \boldsymbol{S}(n-1)$.

A SCP from the gait segment in (1) is added to the shape curve such that the shape frame vector from $\boldsymbol{P}_{n-1}$ to the new SCP equals the vector from the previous to the new SCP in the gait segment. In other words, when SCP $j \in \{1, \ldots, k-1\}$ from the gait segment is added to the shape curve, its global frame coordinates $\boldsymbol{P}_{\text{new}}$ are

$$\boldsymbol{P}_{\text{new}} = \boldsymbol{P}_{n-1} + \boldsymbol{R}_z\left(\psi_s\right)\left(\boldsymbol{P}_j^{\text{GS}} - \boldsymbol{P}_{j-1}^{\text{GS}}\right) \tag{2}$$

where

$$\boldsymbol{R}_z\left(\psi_s\right) = \begin{bmatrix} \cos\psi_s & -\sin\psi_s & 0 \\ \sin\psi_s & \cos\psi_s & 0 \\ 0 & 0 & 1 \end{bmatrix} \tag{3}$$

is the rotation matrix from the shape frame to the global frame. Note that after all k SCPs from the gait segment have been added to the shape curve, the process starts over from the first SCP.

3) The Virtual Snake Robot: The VSR has similar kinematics as the physical robot (i.e. N links of length l) and is aligned along the shape curve by placing each joint center on the curve. As shown in Fig. 4, the resulting angle of link $j \in \{1, \ldots, N\}$ is denoted by θ_j^{VS}, where superscript 'VS' is short for *virtual snake*. Furthermore, we denote the shape curve parameter of joint $j \in \{0, \ldots, N\}$ by s_j, where s_0 is the shape curve parameter of the tail tip, s_1 is the parameter of the first joint, and $s_N = s_{\text{head}}$ is the parameter of the head tip.

In order to generate joint reference angles corresponding to the cyclic gait pattern, the VSR is simply progressed forward along the shape curve at some desired velocity denoted by v^{VS}. This progression is achieved by manipulating the control input s_{head} (i.e. the shape curve location of the head tip) such that $\left|\dot{\boldsymbol{S}}(s_{\text{head}})\right| = v^{\text{VS}}$. Every time the VSR reaches the end of the shape curve, a new SCP is added to the curve according to (2).

4) The Heading Controller: In order to steer the physical snake robot towards the desired straight path, we employ the Line-of-Sight (LOS) guidance law [2]

$$\overline{\theta}_{\text{ref}} = -\arctan\left(\frac{p_y}{\Delta}\right) \tag{4}$$

where p_y is the cross-track error and $\Delta > 0$ is a design parameter referred to as the *look-ahead distance*. The heading reference angle $\overline{\theta}_{\text{ref}}$ corresponds to the orientation of the robot when it is headed towards the point that is located a distance Δ ahead of itself along the desired path.

In order to control the heading $\overline{\theta}$ of the physical robot according to $\overline{\theta}_{\text{ref}}$, we choose to manipulate the shape frame angle ψ_s. Since, by (2), this angle determines the direction in which the shape curve is developed, we conjecture that a rotation of the shape frame will introduce a similiar change in the heading of the physical robot. To this end, we align the shape frame with the heading of the VSR, which we define as $\overline{\theta}^{\text{VS}} = \frac{1}{N}\sum_{j=1}^{N}\theta_j^{\text{VS}}$, and we steer the physical robot by adjusting ψ_s according to the control law

$$\psi_s = \overline{\theta}^{\text{VS}} + k_\psi\left(\overline{\theta}_{\text{ref}} - \overline{\theta}\right) \tag{5}$$

where $k_\psi > 0$ is the gain of the heading controller.

Remark 5: The shape frame orientation has no influence on existing SCPs in the shape curve, which means that directional control according to (5) is only performed when a new SCP is added according to (2).

5) The Control Input for the Physical Snake Robot: The joint angles of the aligned VSR are continuously used as joint reference angles for the physical robot. Consequently, the reference angle of joint $j \in \{1, \ldots, N-1\}$ of the physical robot is

$$\phi_{j,\text{ref}} = \theta_j^{\text{VS}} - \theta_{j+1}^{\text{VS}} \tag{6}$$

and we choose the motor torque u_j at joint j according to the PD controller

$$u_j = k_p\left(\phi_{j,\text{ref}} - \phi_j\right) - k_d\dot{\phi}_j \tag{7}$$

where $k_p > 0$ and $k_d > 0$ are controller gains.

Remark 6: A formal analysis of the complete path following controller is a topic of future work.

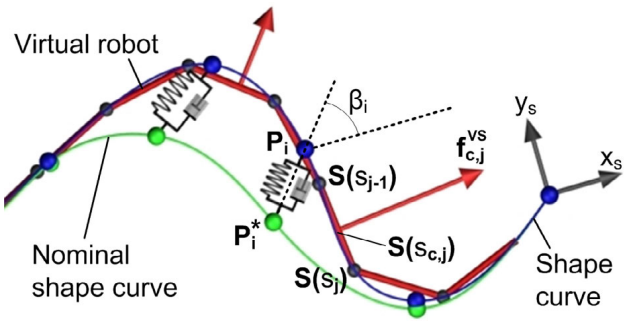

Fig. 5. The compliance of the shape curve is achieved by assigning mass-spring-damper dynamics to the SCPs.

TABLE III
PARAMETERS OF THE COMPLIANCE CONTROLLER.

Symbol	Description
$\boldsymbol{P}_i^* \in \mathbb{R}^3$	Nominal (initial) coordinates of the ith SCP.
$\beta_i \in \mathbb{R}$	Angle of the vector $\boldsymbol{P}_i - \boldsymbol{P}_i^*$ w.r.t. the x_s axis.
$m_{\text{SCP}} \in \mathbb{R}$	Virtual mass of an SCP.
$k_{\text{SCP}}(\beta) \in \mathbb{R}$	Spring coefficient profile for the SCPs.
$d_{\text{SCP}} \in \mathbb{R}$	Damping coefficient for the SCPs.
$a_{\text{SCP}}(\overline{s}) \in \mathbb{R}$	Adaptation profile for the SCPs.
$\boldsymbol{f}_{\text{c},j}, \boldsymbol{f}_{\text{c},j}^{\text{VS}} \in \mathbb{R}^3$	Contact force on link j of the *physical* robot and the VSR, respectively.
$s_{\text{c},j} \in \mathbb{R}$	Shape curve location of the contact force on link j.
$\boldsymbol{F}_{i,j} \in \mathbb{R}^3$	Force on ith SCP due to contact force on link j.

V. Application of the Motion Planning Framework for Compliant Body Shape Control

In this section, we employ the motion planning framework to propose a compliance controller which makes the body shape of a snake robot compliant with respect to contact forces from its environment.

A. Assumptions

We apply the same assumptions as described in Section IV-A. In addition, we assume that the normal direction contact forces on the links are measured, where $\boldsymbol{f}_{\text{c},j}$ is the measured contact force on link $j \in \{1, \ldots, N\}$.

B. Motivation and Overview

Efficient locomotion in cluttered environments requires that the body shape motion is adapted to the geometry of the environment. The motion planning framework proposed in this paper is particularly well suited to tackle this control problem since the body shape of the robot can be controlled quite directly with respect to its environment through the SCP coordinates.

The idea behind the control scheme proposed in this section is illustrated in Fig. 5 and involves assigning mass-spring-damper dynamics to the SCPs of the shape curve. In particular, measured contact forces along the body of the physical snake robot are mapped to the shape curve and displace the SCPs according to their mass-spring-damper dynamics (i.e. the SCPs are compliant). Consequently, the adjusted shape curve automatically adapts the shape of the physical robot to its environment. The control scheme uses the parameters listed in Table III.

C. The Compliance Controller

1) Mapping Contact Forces to the Shape Curve: The measured contact force on link $j \in \{1, \ldots, N\}$ of the physical snake robot is given by $\boldsymbol{f}_{\text{c},j}$ and acts in the normal direction of the link. We map this contact force to the shape curve by assuming that a similar contact force acts in the center and normal direction of link j of the VSR. In particular, we denote the shape curve parameter of this force by $s_{\text{c},j}$. Since the force shall act in the center of link j of the VSR and since the shape curve parameter of the joint at each end of link j is given by s_{j-1} and s_j, respectively (see Section IV-C.3), we define the shape curve parameter of the contact force as

$$s_{\text{c},j} = \frac{1}{2}\left(s_{j-1} + s_j\right) \tag{8}$$

The resulting force mapped to the shape curve is denoted by $\boldsymbol{f}_{\text{c},j}^{\text{VS}}$. Since the force is normal to link j of the VSR, whose link angle is θ_j^{VS}, we have that

$$\boldsymbol{f}_{\text{c},j}^{\text{VS}} = \boldsymbol{R}_z\left(\theta_j^{\text{VS}} - \theta_j\right)\boldsymbol{f}_{\text{c},j} \tag{9}$$

where the rotation matrix $\boldsymbol{R}_z(\theta_j^{\text{VS}} - \theta_j)$ is defined in (3) and rotates the force $\boldsymbol{f}_{\text{c},j}$ so that it points in the normal direction of link j of the VSR.

2) Mapping Shape Curve Forces to the SCPs: The effect of the contact forces on the SCPs is defined by an adaptation profile $a_{\text{SCP}}(\overline{s})$. The adaptation profile is identical for all SCPs and is simply a scalar function that scales the force applied to a SCP based on the shape curve parameter distance $\overline{s}$ from the SCP to the force. In particular, since the shape curve parameter of the contact force on link j is $s_{\text{c},j}$, its curve parameter distance to the ith SCP is

$$\overline{s} = i - s_{\text{c},j} \tag{10}$$

since the curve parameter of the ith SCP by definition is i. Consequently, the resulting force acting on the ith SCP due to the contact force on link j is given by

$$\boldsymbol{F}_{i,j} = a_{\text{SCP}}\left(i - s_{\text{c},j}\right)\boldsymbol{f}_{\text{c},j}^{\text{VS}} \tag{11}$$

where $\boldsymbol{f}_{\text{c},j}^{\text{VS}}$ is defined in (9).

The adaptation profile is a key control design parameter. If $a_{\text{SCP}}(\overline{s}) = 0$, then no environment adaptation occurs. A natural choice is to choose the profile such that $a_{\text{SCP}}(\overline{s}) \in [0, 1]$, and such that the scaling is high for small $\overline{s}$ (i.e. for SCPs that are close to the contact force) and small/zero for large $\overline{s}$. With this approach, a contact force will induce adaptive behaviour of the body shape close to the applied force, while more distant parts of the body will not be affected by the force. Such local adaptive behaviour is also displayed by biological snakes [12]. To this end, we propose that the adaptation profile is defined according to the exponential function

$$a_{\text{SCP}}(\overline{s}) = e^{-(k_a\overline{s}+\delta)^2} \tag{12}$$

which satisfies $a_{\text{SCP}}(\overline{s}) \in [0, 1]$, and where k_a and δ are design parameters. The effect of this adaptation profile on

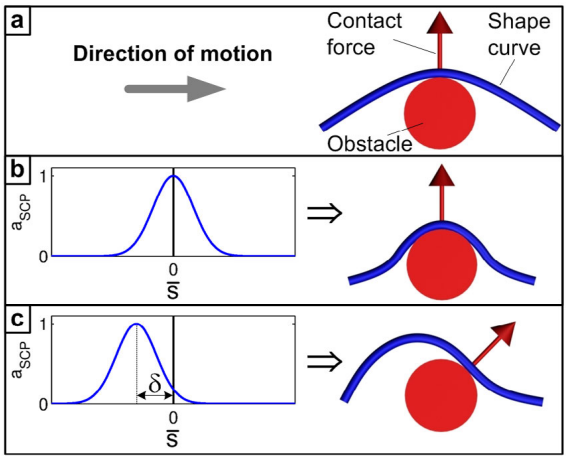

Fig. 6. A contact force acting along the shape curve (a), and the resulting adapted shape curve using (12) with $\delta = 0$ (b) and $\delta > 0$ (c).

the shape curve is illustrated in Fig. 6, which shows that δ offsets the compliance location with respect to the contact force. In particular, a SCP will get the largest influence of the force on link j if its shape curve parameter is $s_{c,j} - \delta/k_a$. We conjecture that *lateral inhibition* [1] is achieved for $\delta = 0$ (Fig. 6(b)), while rotation of the contact force towards the forward direction is achieved for $\delta > 0$ (Fig. 6(c)).

3) The Compliance Dynamics: The compliant behaviour of the shape curve, which we introduce to adapt the body of the robot to its environment, is achieved by assigning mass-spring-damper dynamics to the SCPs. In particular, each SCP $i \in \{0, \ldots, n-1\}$ is assigned a virtual mass m_{SCP}. Furthermore, a virtual spring-damper is connected between its current coordinates $\boldsymbol{P}_i$ and its nominal (initial) coordinates $\boldsymbol{P}_i^*$, i.e. the coordinates of the SCP when it was first added to the shape curve (see Fig. 5). With this approach, a SCP will be compliant around its initial coordinate and, consequently, the shape curve will be compliant around the gait pattern encoded in the gait segment (see Section IV-C.1). The spring and damping coefficient of the SCPs are denoted by k_{SCP} and d_{SCP}, respectively.

In the following, we elaborate on the choice of spring stiffness k_{SCP}. A contact force acting in the forward direction of the snake robot contributes positively to its propulsion, while contact forces acting in the opposite direction are obstructive. For this reason, the adaptive behaviour of the shape curve should depend on the direction of the contact force with respect to the forward direction of motion. We achieve such directionally dependent compliance by choosing a directionally dependent spring stiffness $k_{\text{SCP}}(\beta)$, where β is the direction in which the spring is displaced. As illustrated in Fig. 5, the direction in which the ith SCP is displaced is denoted by the angle β_i and is defined with respect to the x_s axis of the shape frame. We define β_i with respect to the shape frame since the x_s axis is aligned with the heading of the VSR (see Section IV-C.4), which means that the x_s axis defines the direction of propulsive contact forces. A natural choice is to make the shape curve highly compliant for obstructive contact forces and stiff or less compliant for propulsive contact forces. To this end, we propose that the spring coefficient profile is defined according to the exponential function

$$k_{\text{SCP}}(\beta) = k_1 + k_2 e^{-\beta^2} \tag{13}$$

which gives a spring stiffness of $k_1 + k_2$ for spring extension along the forward direction of motion ($\beta = 0$), and which decreases towards k_1 for increasing spring extension angles.

From the above discussion, we can now state the compliance dynamics of the ith SCP of the shape curve as

$$m_{\text{SCP}}\ddot{\boldsymbol{P}}_i + d_{\text{SCP}}\dot{\boldsymbol{P}}_i + k_{\text{SCP}}(\beta_i)(\boldsymbol{P}_i - \boldsymbol{P}_i^*) = \sum_{j=1}^{N} \boldsymbol{F}_{i,j} \tag{14}$$

where $i \in \{0, \ldots, n-1\}$, $\ddot{\boldsymbol{P}}_i$ and $\dot{\boldsymbol{P}}_i$ are the acceleration and velocity of the SCP, respectively, $(\boldsymbol{P}_i - \boldsymbol{P}_i^*)$ is the extension of the virtual spring, and the summation term on the right-hand side gives the total force on the SCP from the contact forces on all N links of the snake robot according to (11). For an appropriately defined adaptation profile $a_{\text{SCP}}(\bar{s})$ and spring coefficient profile $k_{\text{SCP}}(\beta)$, we conjecture that the shape dynamics in (14) will automatically adapt the locomotion of a snake robot to its environment.

VI. Simulation Study

This section presents simulation results which illustrate the performance of the path following controller from Section IV combined with the compliance controller from Section V.

A. Simulation Parameters

1) Model Parameters: The model of the snake robot presented in Section II was implemented in *Matlab R2011a*. The parameters of the robot were $N = 11$, $l = 16$ cm, $m = 0.6$ kg, and $J = 0.0013$ kgm^2. Circular obstacles measuring 10 cm in diameter were placed in a random fashion in the environment of the snake robot. The ground and obstacle friction coefficients were $\mu = 0.2$ and $\mu_o = 0.25$, respectively. The initial link angles were zero and the initial CM position was $\boldsymbol{p} = (0, 1)$, i.e. the robot was initially placed 1 m away from the desired path (the global x axis) with its heading parallel to the path.

2) Control Parameters: The motion planning framework was implemented in Matlab alongside the mathematical model of the snake robot. The shape curve was constructed using a *piecewise cubic hermite interpolating polynomial* [13], which is achieved in Matlab using the function '*pchip*'. This interpolation method was chosen since it creates smooth curves which do not overshoot the SCPs.

With reference to Section IV, the gain and look-ahead distance of the heading controller were $k_\psi = 1$ and $\Delta = lN/2 = 0.88$ m, respectively, and the joint angle controller gains were $k_p = 4$ and $k_d = 1$. The progression velocity of the VSR along the shape curve was $v^{\text{VS}} = 20$ cm/s. The gait segment was defined according to the $k = 9$ SCPs plotted in Fig. 8(a).

The compliance controller in (14) was implemented using the adaptation profile defined by (12) with $k_a = 1.4$ and $\delta = 1$. The profile is plotted in Fig. 8(b) and we chose $\delta > 0$ to achieve the propulsive effect illustrated in Fig. 6(c). The virtual mass and damping coefficient of the SCPs were $m_{\text{SCP}} = 1$ kg and $d_{\text{SCP}} = 20$, respectively. The spring coefficient profile was defined according to (13) with $k_1 = 30$ and $k_2 = 100$, and is plotted in Fig. 8(c).

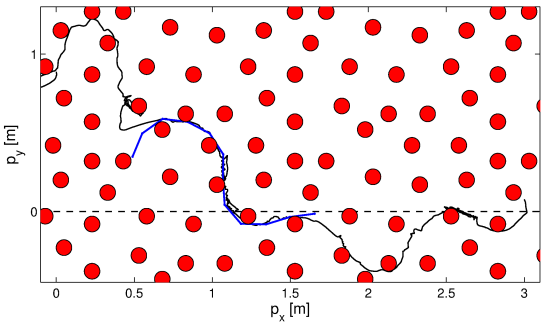

(a) The path of the center link (link 6).

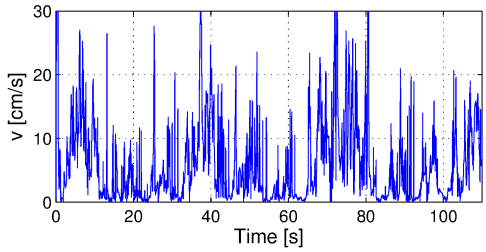

(b) Locomotion velocity, v.

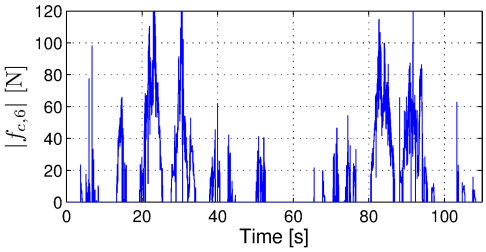

(c) Contact force on link 6, $|f_{c,6}|$.

Fig. 7. Simulation of path following *without* environment adaptation.

B. Simulation Results

To show the importance of environment adaptation during snake locomotion, the path following controller was first simulated *without* body compliance, i.e. with the adaptation profile $a_{\text{SCP}}(\bar{s}) = 0$. The path of the center link of the physical snake robot (link 6) is plotted in Fig. 7(a), where the red circles indicate the obstacles, the dotted black line indicates the desired straight path, and where the shape and position of the robot are shown in blue at $t = 50$ s. Furthermore, Fig. 7(b) shows the locomotion velocity of the robot, which we define as $v = \sqrt{\dot{p}_x^2 + \dot{p}_y^2}$, and Fig. 7(c) shows the magnitude of the contact forces on the center link, i.e. $|f_{c,6}|$, which is representative for the contact forces on the remaining links. We see from Fig. 7(a) that the robot managed to reach the desired path. However, we see from Fig. 7(b) that the displacement of the robot was very slow (at periods close to zero), and from Fig. 7(c) that the motion was very energy inefficient due to large contact forces in the normal direction of the links, which imply large obstacle friction forces in their tangential direction.

Next, we consider the corresponding simulation results *with* body compliance. Fig. 9 shows the path of the robot and also its shape and position at $t = 20$ s, 60 s, and 90 s, respectively. Furthermore, Fig. 10 shows (a) the cross-track error, (b) the heading, (c) the locomotion velocity, and (d) the center link contact forces. Moreover, Fig. 10(e)-(f) illustrate the function of the compliance controller by showing the VSR and the physical robot at $t = 49$ s. In Fig. 10(e), lines are drawn between the nominal and adapted SCPs to indicate the extension of the springs.

There is a significant improvement in the locomotion efficiency when body shape compliance is present. In particular, we see from Fig. 9 that the distance travelled by the robot is more than trippeled compared to in Fig. 7(a), and from Fig. 10(d) that the magnitudes of the obstacle contact forces are significantly reduced compared to the forces in Fig. 7(c). In summary, the proposed control strategy successfully steered the snake robot towards and along the desired straight path in the obstacle environment.

VII. Conclusions

This paper has presented a general motion planning framework for body shape control of snake robots using shape control points. The framework was employed to formulate a controller which enables a snake robot to track straight paths, and also to achieve body shape compliance in environments with obstacles by assigning mass-spring-damper dynamics to the shape control points. The successful performance of the control strategies was illustrated with simulation results.

References

[1] S. Hirose, *Biologically Inspired Robots: Snake-Like Locomotors and Manipulators*. Oxford: Oxford University Press, 1993.

[2] P. Liljebäck, K. Y. Pettersen, Ø. Stavdahl, and J. T. Gravdahl, *Snake Robots - Modelling, Mechatronics, and Control*, ser. Advances in Industrial Control. Springer, 2013.

[3] P. Prautsch, T. Mita, and T. Iwasaki, "Analysis and control of a gait of snake robot," *Trans. Institute of Electrical Engineers of Japan*, vol. 120-D, no. 3, pp. 372–381, 2000.

[4] S. Ma, "Analysis of creeping locomotion of a snake-like robot," *Adv. Robotics*, vol. 15, no. 2, pp. 205–224, 2001.

[5] M. Saito, M. Fukaya, and T. Iwasaki, "Serpentine locomotion with robotic snakes," *IEEE Contr. Syst. Mag.*, vol. 22, no. 1, pp. 64–81, February 2002.

[6] Z. Y. Bayraktaroglu, "Snake-like locomotion: Experimentations with a biologically inspired wheel-less snake robot," *Mechanism and Machine Theory*, vol. 44, no. 3, pp. 591–602, 2008.

[7] T. Sato, T. Kano, R. Kobayashi, and A. Ishiguro, "Snake-like robot driven by decentralized control scheme for scaffold-based locomotion," in *Proc. IEEE/RSJ Int. Conf. Intelligent Robots and Systems (IROS)*, 2012, pp. 132–138.

[8] T. Kamegawa, R. Kuroki, M. Travers, and H. Choset, "Proposal of earli for the snake robot's obstacle aided locomotion," in *IEEE Int. Symp. Safety, Security, and Rescue Robotics (SSRR)*, 2012, pp. 1–6.

[9] D. Rollinson and H. Choset, "Gait-based compliant control for snake robots," in *Proc. IEEE Int. Conf. Robotics and Automation*, 2013, pp. 5123–5128.

[10] P. Liljebäck, K. Y. Pettersen, Ø. Stavdahl, and J. T. Gravdahl, "A control framework for snake robot locomotion based on shape control points interconnected by Bézier curves," in *Proc. IEEE/RSJ Int. Conf. on Intelligent Robots and Systems*, 2012, pp. 3111–3118.

[11] ——, "Hybrid modelling and control of obstacle-aided snake robot locomotion," *IEEE Trans. Robotics*, vol. 26, no. 5, pp. 781–799, Oct 2010.

[12] B. Moon and C. Gans, "Kinematics, muscular activity and propulsion in gopher snakes," *Journal of Experimental Biology*, vol. 201, pp. 2669–2684, 1998.

[13] F. N. Fritsch and R. E. Carlson, "Monotone piecewise cubic interpolation," *SIAM J. Numerical Analysis*, vol. 17, no. 2, pp. 238–246, 1980.

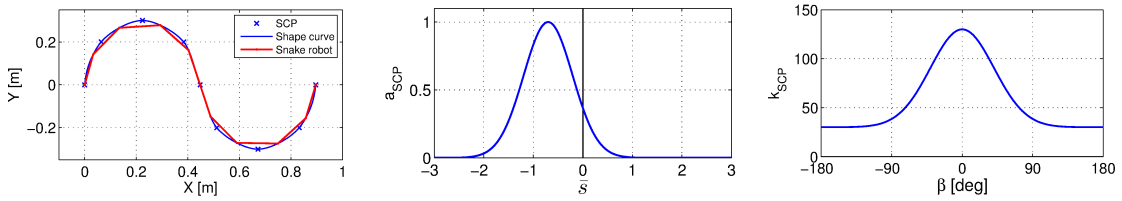

(a) The gait segment. (b) The adaptation profile. (c) The spring profile.

Fig. 8. The gait segment, adaptation profile, and spring coefficient profile used in the simulation.

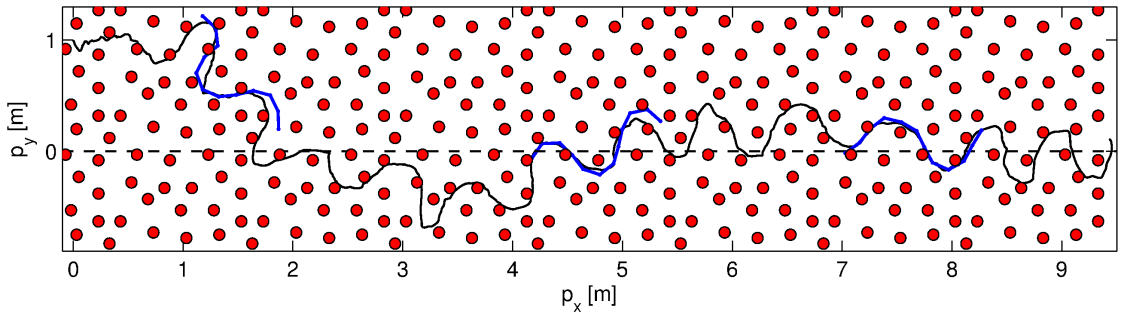

Fig. 9. The path of the center link (link 6) of the snake robot during path following *with* environment adaptation.

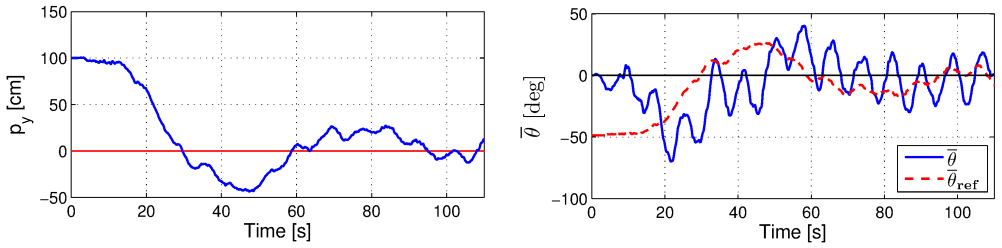

(a) Cross-track error, p_y. (b) Heading angle, $\overline{\theta}$.

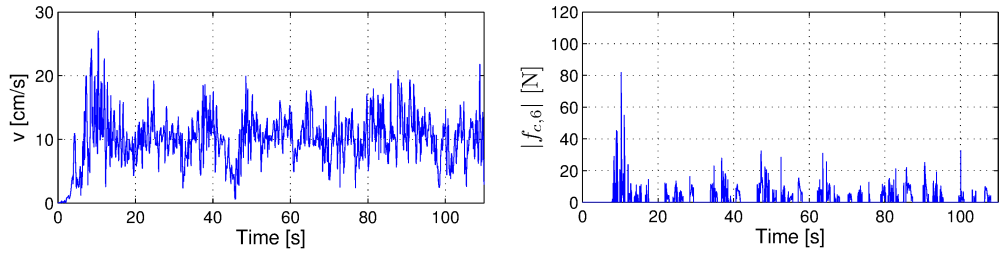

(c) Locomotion velocity, v. (d) Contact force on link 6, $|f_c, 6|$.

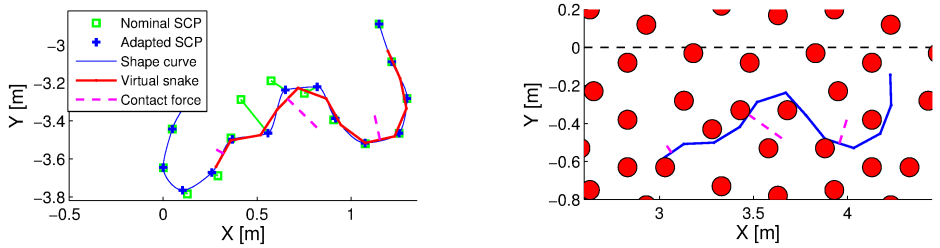

(e) VSR at $t = 49$ s. (f) Physical robot at $t = 49$ s.

Fig. 10. The cross-track error, heading, velocity, and contact force amplitudes of the snake robot during path following *with* environment adaptation.